Biophysical Journal
Article

Biophysical Society

DLITE Uses Cell-Cell Interface Movement to Better Infer Cell-Cell Tensions

Ritvik Vasan,[1] Mary M. Maleckar,[2] C. David Williams,[2,*] and Padmini Rangamani[1,*]
[1]Department of Mechanical and Aerospace Engineering, University of California, San Diego, San Diego, California and [2]Allen Institute for Cell Science, Seattle, Washington

ABSTRACT Cell shapes and connectivities evolve over time as the colony changes shape or embryos develop. Shapes of intercellular interfaces are closely coupled with the forces resulting from actomyosin interactions, membrane tension, or cell-cell adhesions. Although it is possible to computationally infer cell-cell forces from a mechanical model of collective cell behavior, doing so for temporally evolving forces in a manner robust to digitization difficulties is challenging. Here, we introduce a method for dynamic local intercellular tension estimation (DLITE) that infers such evolution in temporal force with less sensitivity to digitization ambiguities or errors. This method builds upon previous work on single time points (cellular force-inference toolkit). We validate our method using synthetic geometries. DLITE's inferred cell colony tension evolutions correlate better with ground truth for these synthetic geometries as compared to tension values inferred from methods that consider each time point in isolation. We introduce cell connectivity errors, angle estimate errors, connection mislocalization, and connection topological changes to synthetic data and show that DLITE has reduced sensitivity to these conditions. Finally, we apply DLITE to time series of human-induced pluripotent stem cell colonies with endogenously expressed GFP-tagged zonulae occludentes-1. We show that DLITE offers improved stability in the inference of cell-cell tensions and supports a correlation between the dynamics of cell-cell forces and colony rearrangement.

SIGNIFICANCE Cell-cell tensions play a key role in the dynamics of evolving tissue morphogenesis. Mathematical modeling tools have aided in understanding of the role of cell-cell adhesion in tissue organization. In particular, recent modeling studies have shown that an inferential approach can estimate tension distributions in a single image of a cell monolayer (cellular force-inference toolkit). Building on these efforts, here, we include the dynamics of monolayer morphogenesis in the estimation of cell-cell tensions. Such a formulation, named dynamic local intercellular tension estimation, performs better across time in both synthetic geometries and time series of human-induced pluripotent stem cell colonies with endogenously expressed GFP-tagged zonulae occludentes-1. We propose that methods such as this can further elucidate the physical mechanisms that drive morphogenesis.

INTRODUCTION

Cell shape, forces, and function are closely related (1–4). Cell shape is known to affect intracellular organization and transmission of cytoskeletal forces (5–7). In particular, cell membrane tension plays an important role in connecting cell shape and cellular function. For example, cell membrane tension partially governs processes ranging from intracellular endocytic bud morphology during trafficking (8) to tissue-level remodeling events such as wound healing (9), development (10), expansion (11), migration (12,13), and cancer invasion (14). Mechanical rearrangement of the cells and tissues occurs as cells transmit these forces across the membrane (15) and cell-cell adhesion complexes such as adherens and tight junctions (16,17). These apical cortical complexes (18) depend on the activity of the actomyosin cytoskeleton (19,20). The mechanotransduction of intercellular forces can alter and regulate biochemical signaling pathways (21,22) with force and deformation at a particular time point, partially regulating future forces and deformations.

Force-mediated collective behaviors are crucial for the dynamics of tissue reshaping. This is commonly evidenced by apoptosis in cell cultures or by the intercalation

Submitted May 1, 2019, and accepted for publication September 23, 2019.
*Correspondence: cdavew@alleninstitute.org or padmini.rangamani@eng.ucsd.edu
Editor: Vivek Shenoy.
https://doi.org/10.1016/j.bpj.2019.09.034

and extrusion of cells during development (23,24). We can examine the role of tension in tissue remodeling using direct force-measurement techniques such as atomic force microscopy or micropipette aspiration (25–27); we direct the reader to (25) for a comprehensive review for force-measurement methods. These direct measurement techniques offer precise force characterization in cells and tissues but perturb the actomyosin network (28,29). As a result, these methods can alter the force responses of the system at subsequent time points, limiting longitudinal insight. Alternative optical measurement techniques that use Förster resonance energy transfer tension probes or traction force microscopy can assay force (30–32) without the mechanical disruption associated with direct measurements (33). These optical approaches can be applied across extended periods but, like the previous physical techniques, they can be difficult to implement in a high-throughput context. Indeed, traction force microscopy is the most widely used method for measuring force dynamics in processes like migration (34), differentiation (35), and adhesion maturation (36). Förster resonance energy transfer probes are useful to estimate molecular-scale forces localized to any protein of interest (31). However, there has been an exponential increase in imaging data for cells, which calls for inference methods that are purely data-driven to estimate forces. Thus, complementary to experimental approaches, force inference from the geometry of the cell boundary can allow for the estimation of normalized tensions solely from images of labeled confluent cells without further condition requirements.

Intercellular forces can be inferred at cell-cell interfaces using a mechanical model, predicated on the assumption that forces are balanced where multiple cell-cell interfaces meet (37–39). These mechanical models cover a range of complexities, assumptions, and use cases (40). Here, we focus on the representation of tensions in a two-dimensional (2D) plane of curved edges digitized from the apical interfaces of a confluent cell colony (Fig. 1, *A* and *B*). We build upon previous representations of this system (37,38,41–43), notably that used in the cellular force-inference toolkit (CellFIT) (37), and develop an alternate problem formulation that treats tension estimation as a temporally evolving problem, borrowing information from previous time points to increase model prediction stability and boost resistance to ambiguities or errors that arise during the digitization process (Fig. 1 *C*). This provides a nondisruptive means to infer intercellular forces in time-lapse imaging of cell colonies. We term this technique dynamic local intercellular tension estimation (DLITE). Here, we validate DLITE against a range of synthetic data for which known tension ground truths are available and use it to predict tensions in time series of human-induced pluripotent stem (hIPS) cell lines with the endogenously green fluorescent protein (GFP)-labeled tight junction protein ZO-1.

METHODS

Assumptions

We employed a curvilinear description of a cell colony by defining it as a directed planar graph comprising cells (c), edges (e), and nodes (n) (Fig. 1 *B*; for more details, see the Supporting Materials and Methods and (37,44)). Forces exerted by the actomyosin cortex result in tangential stresses in the form of tension (t) along an edge. Cells resist deformation by means of a normal stress exerted as pressure (p) inside every cell. Along each edge, we assumed that the interfacial tensions are homogeneous along the length of the edge and that the intracellular pressures are uniform within a cell. This assumption is important to keep our model tractable and to avoid using a constitutive equation that governs the stress-strain relationships of the colony. At the length scale of the whole cell, we ignored membrane bending and assumed that edge tensions and cell pressures exclusively govern cell shape. We assumed viscous forces to be negligible and therefore assumed colony shape as quasistatic (i.e., at each time point, the colony is in mechanical equilibrium).

Governing equations and system specification

A general force balance at every node in a colony can be written as follows:

$$n_{\text{residual}} = \underbrace{\left| \sum_{i=1}^{e_n} t_i v_i \right|}_{\text{(tension balance per node)}}, \tag{1}$$

where n is a node, t and v represent the tension/tangential stress and local tangent unit vector of an edge connected to node n, respectively, e_n is the number of edges connected to node n, and n_{residual} is the magnitude of the resultant tension vector coming into a node (ideally 0). This notation is shown in Fig. 1 *B*. This equation applies when employing a curvilinear description of the tissue and applies to a node that is both connected to at least three edges and is in mechanical equilibrium (37). The tension balance across multiple nodes can be written as a system of equations given as follows:

$$G_T T = 0, \tag{2}$$

where G_T is a matrix of edge tension coefficients, and T is an array of edge tension magnitudes. CellFIT evaluates edge tensions via inversion of a constrained tension matrix G_T (Eq. 7), the sensitivity of which depends on its condition number κ. The pressure difference between adjacent cells can be estimated using Laplace's law as follows:

$$e_{\text{residual}} = \underbrace{p_i - p_j - \frac{t}{r}}_{\text{(pressure balance per edge)}}, \tag{3}$$

where e is an edge, p_i and p_j are the pressure of adjacent cells i and j, respectively, and e_{residual} is the residual error from the pressure balance. Here, t and r represent the tension and radius of the interfacial edge e. The system of equations for tension and pressure are generally overdetermined; there is no unique solution to this system (37). Therefore, we can only infer the relative distribution of tensions from the shape of the edges and not the absolute values.

To compute the dynamics of cell-cell forces, we reformulated the tension balance (Eq. 1) as a local optimization problem defined as follows:

$$\underset{t}{\text{minimize}}\, f(t) = \sum_{j=1}^{N} \left(n_{\text{j,residual}} + \underbrace{\frac{n_{\text{j,residual}}}{\sum_{i=1}^{e_{n_j}} |t_i v_i|}}_{\text{regularizer}} \right), \tag{4}$$

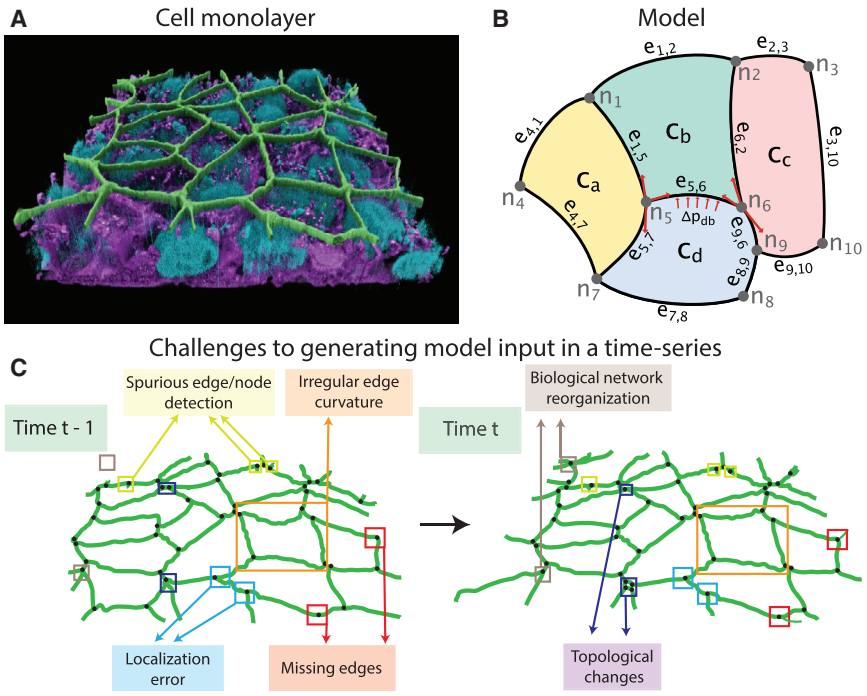

FIGURE 1 A 3D cell view of tight junction location, how this is represented in the model, and the challenges in doing so. (*A*) A 3D view of tight junctions in human-induced pluripotent stem (hIPS) cells from the Allen Cell Explorer (*green*: tight junctions; *purple*: membrane; *blue*: nucleus). We infer cell shape and edge shape from tight junctions as they localize to the tension-bearing apical surface of epithelial-like tissues. (*B*) A schematic of cell-interface representation used in DLITE and CellFIT force-inference techniques (37). A colony is represented as a set of nodes (n), edges (e), and cells (c). Edges are directional. Tension balance occurs at each node (*red arrows* at n_5 and n_6). Pressure difference ($\Delta p_{d,b}$) across a junction is estimated using Laplace's law (*red arrows* at $e_{5,6}$). (*C*) Ambiguities in image segmentation introduce challenges to successful tension inference. Time t−1 shows single time point challenges like spurious edge/node detection, irregular edge curvature, node location errors, and incomplete segmentation. Time t shows time-lapse challenges like biological network reorganization and topological changes. To see this figure in color, go online.

where n_j and e_{n_j} represent the j[th] node and the number of edges connected to node n_j, and N is the total number of nodes in the colony. Here, $n_{j,\text{residual}}$ is the tension residual at a given node (Eq. 1), and the regularizer is the magnitude of the tension residual divided by the sum of the magnitude of the tension vectors acting on that node. Because tension cannot be negative, we set a lower tension bound of zero. In Eq. 4, the regularized term ensures that the system of equations does not converge to the globally trivial solution (tension = 0 along all edges) (45). Such a formulation does not require inversion of G_T (Eq. 2). Pressure in each cell was computed using the equation as follows:

$$\underset{p}{\text{minimize}} \quad g(p) = \sum_{j=1}^{E} e_{j,\text{residual}}^2, \tag{5}$$

where E is the total number of edges in the colony, and e_j is the residual error from the pressure balance at the j[th] edge. Tension and pressure solutions were normalized to an average of 1 and 0, respectively, similar to previous work (37–39). In contrast to previous methods, DLITE uses the values of tension at each edge and pressure in each cell from the previous time point as an initial guess for the current time point. This mode of time stepping in the optimization procedure enables us to use information from previous time points to predict the values of tension and pressure at the current time point and forms the basis of DLITE's improved performance across time series. Our model optimization pipeline was implemented using SciPy's unconstrained optimization algorithm "Limited-memory Broyden–Fletcher–Goldfarb–Shanno (L-BFGS)" (46). The global optimization technique "Basinhopping" was used to seek a global minimum solution at the first time point (47).

Tracking nodes and edges

An essential distinguishing characteristic of DLITE is the ability to provide an initial guess for each edge tension and each cell pressure, allowing us to incorporate a time history of cell-cell forces. However, this requires node, edge, and cell tracking over time. To implement tracking, we first assign labels to nodes, edges, and cells at the initial time point. Then, nodes are tracked by assigning the same label to the closest node at the next time point. Edges are tracked by comparing edge angles connected to nodes with the same label, and cells are tracked by matching cell centroid locations across time.

Geometries for model validation

Validation of DLITE requires the generation of dynamic 2D geometries with curvilinear edges whose cortical tensions are known. Many standard mathematical models describe the modification of cell shape via applied forces that are either explicitly or implicitly specified. Such models include cellular Potts models (48,49), Vertex models (50,51), and cell-level finite-element models (52–54). Implicit models define an energy function relating the variation of tension and other properties in a 2D monolayer to cell shape. The gradient of this energy function leads to the movement of each vertex. Here, we employ an implicit model using the energy minimization framework Surface Evolver (55), which was designed to model soap films. The energy function (W) was defined as follows:

$$W = \underbrace{\sum_{j=1}^{E} t_j L_j}_{\text{tension energy}} + \underbrace{\sum_{k=1}^{C} p_k A_k}_{\text{pressure energy}}, \tag{6}$$

where t_j, L_j are the tension and length of the j[th] edge and p_k, A_k are the pressure and area of the k[th] cell, respectively. E and C are the total number of edges and cells in the colony (see Supporting Materials and Methods for details). Here, the tension energy represents a net energy contribution caused by adhesion forces that stabilize a cell-cell interface and actomyosin cortical tensions that shorten cell-cell contacts. Pressure was enforced as a Lagrange multiplier for an area constraint. Cell boundaries were free to move along the surface. Such a model outputs a minimum energy configuration through gradient descent, providing ground-truth tensions to which we compare inference model outputs. Although the model utilized here describes a monolayer as a 2D surface embedded in three-dimensional (3D)

space, it is possible to extend this work to 3D, covering the complex 3D structure present in many systems (39).

Sources of error due to digitization

Transforming single- or multichannel z-stacks of cell colonies into a connected network suitable for tension inference requires 1) image preprocessing to produce a binary or otherwise simplified representation, 2) skeletonization, creating a network of 0-width lines connecting nodes at junction points, and 3) postprocessing of the skeletonized representation. Inherent ambiguities in this process introduce several challenges to successful tension inference. Some of these challenges, such as incorrectly detecting an edge, occur in single frames (Fig. 1 *C*, time t−1), whereas others, such as edge tracking across biological network reorganization, are only present in time series data (Fig. 1 *C*, time t). These challenges tend to occur more frequently as digitization is increasingly automated, creating a trade-off between data reliability and throughput.

Code availability

Our code is freely available with Jupyter Notebook tutorials at www.github.com/AllenCellModeling/DLITE with documentation at https://dlite.readthedocs.io/en/latest/. To help with download and installation, we have provided a step-by-step screencast as a Video S7 (also available at: https://vimeo.com/360665873). An example notebook is also provided here: https://github.com/AllenCellModeling/DLITE/blob/master/Notebooks/Example.ipynb.

RESULTS

DLITE is built to use the tension at a specific cell-cell junction at a given time point as an initial guess to calculate tensions at the next time point. This logical progression then allows us to infer forces over time and test the strength of the inference method by correlation to ground-truth values for synthetic geometries. We demonstrate robustness and sensitivity of DLITE by validating it against ground-truth tensions for multiple synthetic geometries, multiple tension perturbations within a colony, connectivity ambiguities at single or multiple time points, curve-fit errors, node location errors, and topological changes like the shrinkage of cell-cell contacts. At each point, we compare predictions to those produced by the state-of-the-art CellFIT technique. We use CellFIT as the benchmark model for comparison and validation as the assumption of curved edges outperforms nearly all previous force-inference models that assume straight edges (38,41–43). We then apply DLITE to videos of skeletonizations of endogenously tagged tight junction ZO-1 (zonulae occludentes-1) in an hIPS cell line and demonstrate improved tension stability in the inference of cell-cell forces during colony dynamics. A comparison of CPU times required to generate each figure is provided in Table 1.

TABLE 1 Comparison of CPU Time for MacBook Pro for CellFIT and DLITE

Figure	CellFIT	DLITE
1. Fig. 2	3 min 25 s	14 min 50 s
2. Fig. 3 *D*	1 min 4 s	8 min 25 s
3. Fig. 5	12 s	1 min 21 s
4. ZO-1 time series 1 (Fig. 7 *A*)	12 s	13 min 4 s
5. ZO-1 time series 2 (Fig. 7 *B*)	14.3 s	18 min 23 s
6. ZO-1 time series 3 (Fig. 7 *C*)	12.6 s	5 min
7. ZO-1 time series 4 (Fig. 8)	13.9 s	17 min 18 s

MacBook Pro specifications were as follows: 2 GHz Intel Core i5 6360U

Validation of DLITE as a dynamic tension-inference tool

We validated DLITE in three steps. First, we compared edge tension and cell pressure solutions obtained using our implementation of the CellFIT algorithm and DLITE to ground truth values in synthetic geometries made available via the current version of CellFIT called ZAZU (Fig. S1). We reimplemented the CellFIT algorithm in Python because the source code of ZAZU is not publicly available. Both our reimplementations of CellFIT (Fig. S1 *B*) and implementation of DLITE (Fig. S1 *C*) perform identically with respect to the ground truth for single frames (Fig. S1 *A*), with an average error of ∼0.02 (Fig. S1 *D*).

Second, to generate a time series of synthetic geometries, we simulated colonies that deformed smoothly across time using Surface Evolver (55). Initial geometries were created from random Voronoi tessellations followed by Lloyd relaxation (56). To generate a time series, we performed multiple Evolver simulations in which the tension of a few randomly selected edges were either increased or decreased between time points (Fig. 2 *A*). Average edge tension at each time point was normalized to 1. We then stripped all tension and pressure information from the resulting shapes and used these shapes as input to our method. Using DLITE and CellFIT separately, we inferred colony forces and compared the two approaches (Fig. 2, *B* and *D*). Initially, both methods performed identically but began to show divergence after three frames. Importantly, we observed that the values of tension predicted using our method remain closer together over time and are better correlated ($r = 0.94$ (DLITE) versus $r = 0.75$ (CellFIT)) to the ground truth (Fig. 2, *B* and *D*). Further, we observed that the variation in tension defined by the change in edge tension over time (denoted as Δtension) using DLITE also correlates better to the ground-truth change in edge tension (Fig. 2 *C*). The improved performance of DLITE at later time points (Fig. S2 *B*) results from DLITE use of information from previous time points to improve tension predictions in the presence of large curve-fit residuals (Fig. S2 *A*), thereby reducing sensitivity to curve-fitting errors. In the absence of an informed prior (i.e., when we use random initial guesses sampled from a random Gaussian distribution at every time point), we observed worse performance of DLITE (Table S1). Colony pressures for the time series in Fig. 2 showed a minor improvement (Fig. S3) because the pressure equations are well conditioned.

Third, to ensure robustness of the performance of DLITE, we tested multiple tension perturbations via different combinations of increasing and decreasing edge tension in the

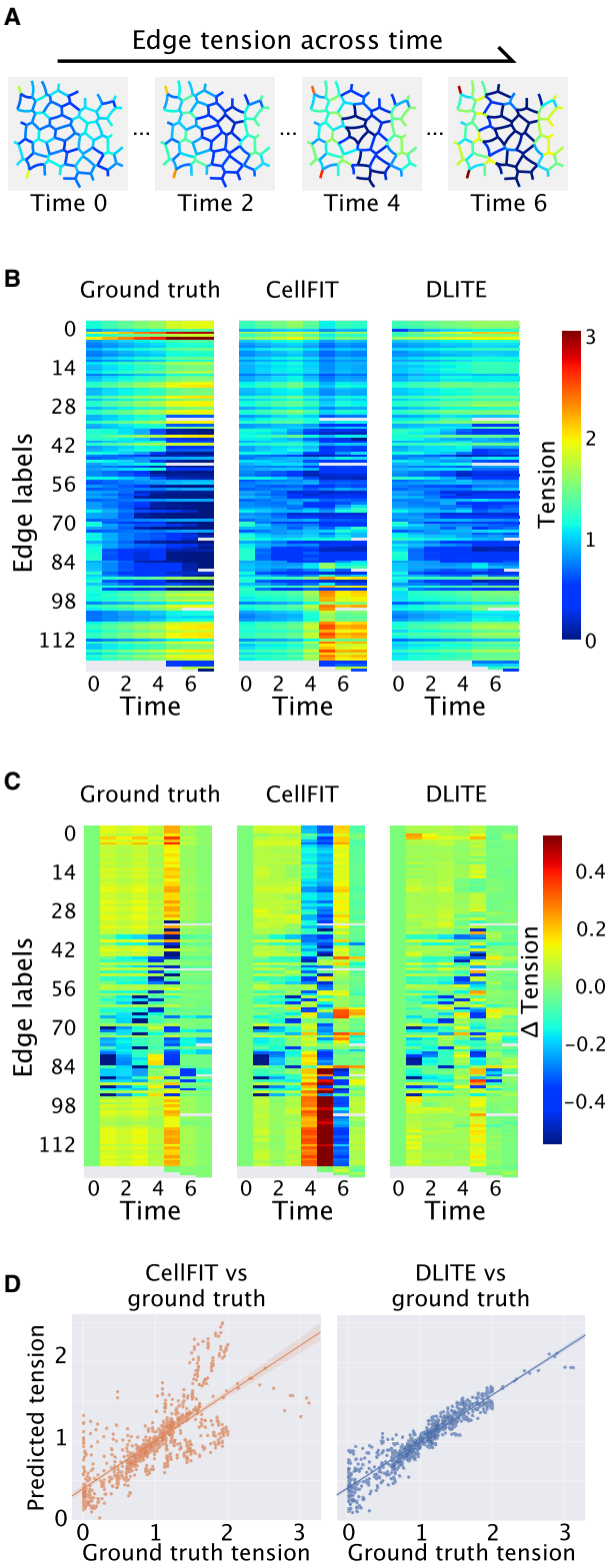

FIGURE 2 Comparison of DLITE and CellFIT force-inference techniques for digitized time series. Synthetic colonies were generated from random Voronoi tessellations and morphed to minimum energy configurations (Eq. 6) using Surface Evolver (55). A random set of edges within the colony were perturbed by decreasing or increasing their tensions, resulting in a new colony structure; repeating this process produced a time series of colony rearrangement. (*A*) A time series of a synthetic colony showing the decrease in tension of 70 edges in the middle of the colony and the increase in tension of 40 edges along the boundary. (*B*) A heat map of dynamic edge tensions for ground truth, CellFIT, and DLITE. (*C*) A heat map of dynamic change (derivative of tension) in edge tensions for ground truth, CellFIT, and DLITE. (*D*) A comparison of inferred versus ground-truth tensions for CellFIT ($r = 0.75$) and DLITE ($r = 0.94$). Here, r is the Pearson's correlation coefficient. To see this figure in color, go online.

same geometry (Fig. S4) and similar perturbations in other randomly generated geometries (Fig. S5). In all cases, we observed equivalent or better correlation of both the tension and change in edge tension with the ground truth using DLITE as compared to CellFIT.

DLITE is robust to digitization ambiguities

The input to a force-inference model is a map of colony shape as a series of curved edges and the nodes where edges join (Fig. 1 *B*). Segmentation transforms image data into information about the isolated geometric structures (57,58). Subsequently, skeletonization methods extract lines that characterize the topology and connectivity of the tension bearing network in the colony. Ambiguities or errors in this mapping present challenges to force-inference techniques that rely on precise colony connectivity and edge tracing (37–39). Some of these conditions are shown in Fig. 1 *C*. New methods have improved the quality and repeatability of predicted network topology and connectivity; both deep learning models and traditional computer vision techniques have made significant advances in 2D/3D biological segmentations (59–62). Despite these advances, current skeletonization methods continue to require semimanual postprocessing because of the ambiguities present in the structures during imaging and errors resulting from the image capturing modalities. This semimanual cleanup becomes increasingly impractical for larger colonies and time series. As a result, we require force-inference techniques robust to errors in mapping a given cell monolayer to a series of interconnected curved edges. As we demonstrate below, our inference method has increased robustness to multiple edge/node mapping errors. Therefore, our method decreases the number of manual corrections required and increases the tractability for inferring forces. Here, we evaluate the effects of edge/node mapping errors on force-inference in a single image and in a time series.

We first analyzed, at a single time point, the effect of a missing intersection between two edges, a commonly occurring connectivity error. As before, we generated a synthetic colony image to initialize the system with known edge tensions. Fig. 3 *A* shows a random Voronoi tessellation generated using Surface Evolver in which 50 edges (out of 330 total) have larger values of tension than others. The ground-truth tensions were the inputs given to Surface Evolver (Fig. 3 *A*). A single edge was deliberately traced

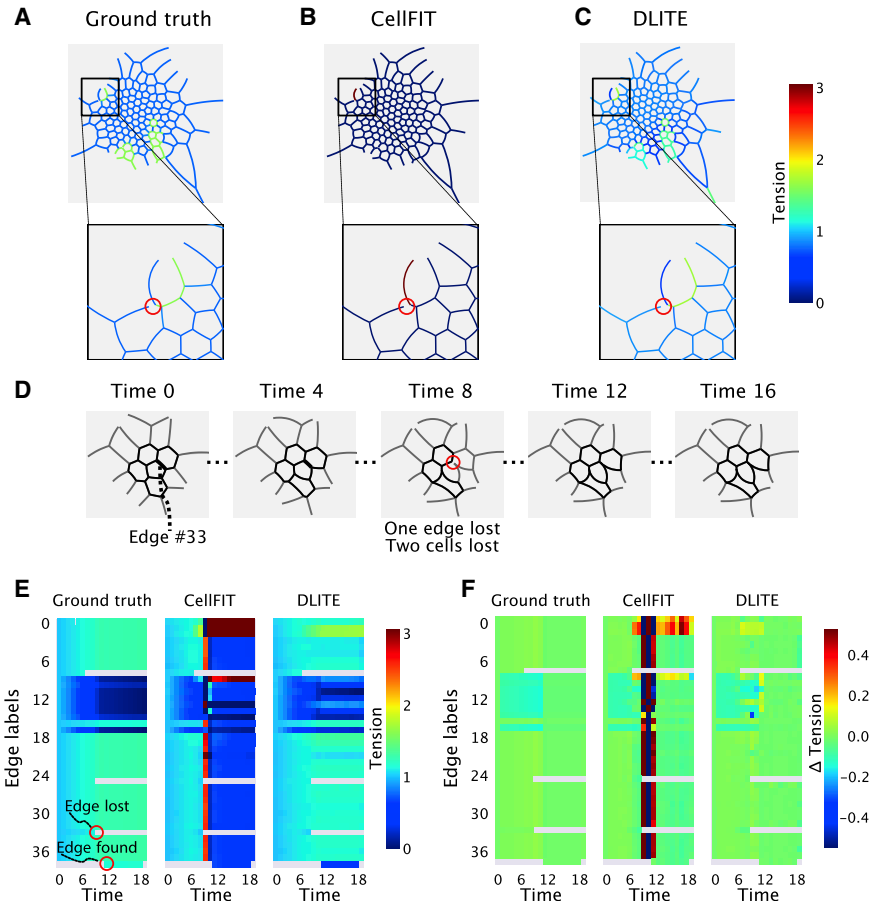

FIGURE 3 Reduced sensitivity to connectivity errors in DLITE. (*A*) Ground-truth tensions for a synthetic geometry containing 330 edges generated used Surface Evolver with a single-edge connectivity error (*circled in red*). (*B*) Edge tensions computed using CellFIT for the geometry in (*A*). (*C*) Edge tensions computed using DLITE for the geometry in (*A*). (*D*) Time series of a synthetic geometry containing 37 edges generated using Surface Evolver with a single-edge connectivity error at time 8 (*circled in red*). This edge is found again in time step 10 (representing a transient encoding error) but treated as a new edge. (*E*) A heat map of dynamic edge tensions for ground truth, CellFIT ($r = 0.14$), and DLITE ($r = 0.87$) for the time series in (*D*). (*F*) A heat map of dynamic change (derivative of tension) in edge tensions for ground truth, CellFIT, and DLITE for the time series in (*D*). To see this figure in color, go online.

incorrectly to introduce a connectivity error (Fig. 3 *A*, *inset*). This error resulted in the loss of a triple junction and loss of cellular integrity. Because the node of interest is now connected to two edges instead of three, we can no longer conduct a tension balance at that location. Such an ill-posed problem results in a singular tension matrix G_T (Eq. 2), implying that CellFIT is unable to infer a correct tension distribution (Fig. 3, *A* and *B*). However, the use of a regularizer in DLITE (Eq. 4) reduces the effect of local tension errors on the global data set. As a result, we find that at a given time point, DLITE is able to provide a good estimate of the tension of the neighboring edges, even in the presence of connectivity errors (Fig. 3 *C*; see also Figs. S6 and S7).

A commonly occurring digitization challenge results from poor estimation of edge curvature due to incorrect values of between-edge angles at a particular node. Errors in curve fitting can lead to poor tension residuals (Eq. 1) or large condition numbers of tension matrices (Eq. 2), which is defined as the ratio of the largest to smallest singular values in the SVD of the given tension matrix. Subsequently, this leads to poor inference of tension (Fig. 2). This is especially problematic when cell-cell junctions are distinctly noncircular, as they commonly are. To simulate this, we generated a time series of synthetic geometries using Surface Evolver such that later time points are distinctly noncircular (Fig. S8 *A*). The large curve-fit residuals at later time points (Fig. S8 *B*) lead to ill-conditioned tension matrices and errors in tension inference (Fig. S8 *C*). However, DLITE uses tension information from previous time points to retain the distribution of tensions and is not poorly scaled by these curve-fit errors (Fig. S8 *C*).

Another major digitization challenge for force-inference models is the accurate determination of node locations. Localization errors in node coordinates also have the downstream impact of changing connected edge curvatures (Fig. 4 *B*). We simulated this type of error by adding levels of Gaussian noise to nodes in a synthetic colony (Fig. 4 *A*, *red nodes*). Noise levels 1 (Fig. 4, *C* and *F*), 2 (Fig. 4, *D* and *G*), and 3 (Fig. 4, *E* and *H*) refer to the Gaussian noise terms with a mean of 0 and SDs of 0.1, 0.5, and 1, respectively. In all cases, we observed equivalent (noise level 1) or improved performance (noise levels 2, 3) when using DLITE compared to CellFIT. Thus, DLITE offers improved quality of tension inference in the presence of ambiguities in node location.

Finally, we considered a class of mapping challenges that are unique to time-series data, that of identification

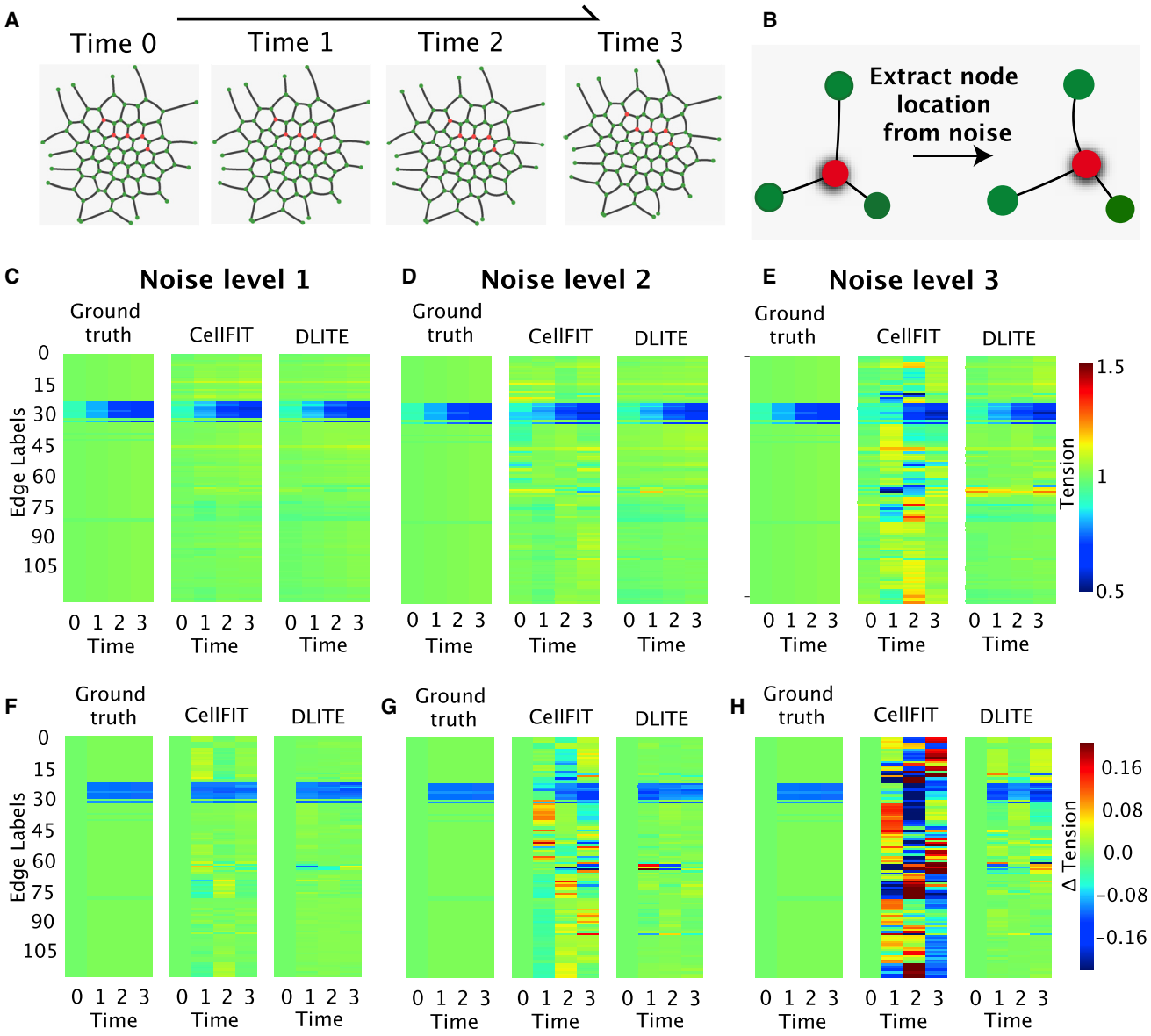

FIGURE 4 Reduced sensitivity to node location errors in DLITE. Noise levels 1, 2, and 3 correspond to random Gaussian noise added to red node locations, all with a mean 0 and SD of 0.1, 0.5, and 1, respectively. Red node coordinates are (480.95, 525.7), (487.76, 536.94), (498.63, 522.1), (524.25, 503.43), and (535.62, 515.97), arranged from left to right. (*A*) A time series of synthetic colony generated using Surface Evolver. The five nodes subject to perturbation with noise are shown in red. (*B*) Change in shape of a single triple junction around the red node in the presence of noise. (*C–E*) A heat map of dynamic edge tensions for ground truth, CellFIT, and DLITE at noise levels 1, 2, and 3, respectively. (*F–H*) A heat map of dynamic change (derivative of tension) in edge tensions for ground truth, CellFIT, and DLITE at noise levels 1, 2, and 3, respectively. To see this figure in color, go online.

of edges from one frame to the next. Misidentification of edges frequently occurs when an edge is lost for a single frame, severing the edge's connection to its previous label. Fig. 3 *D* shows a time series with a missing edge and two missing cells at time point 8. The missing edge leads to the loss of a triple junction and consequently a singular tension matrix (Fig. 3 *E*, CellFIT). For tracking purposes, missing an edge also means that the edge that was being tracked up to that point no longer exists; therefore, a new edge label is assigned. Because edges with new labels do not have an initial tension guess from an identical label at previous time points, these edges are given an initial guess for the value of tension equal to the average initial guess of all edges connected to that edge. By using such a scheme, DLITE can predict tension and Δtension (change in edge tension of an edge label between adjacent time points) that correlates well with the ground truth (Fig. 3, *E* and *F*). Thus, in both images and videos of colonies, we find that use of information from the neighboring region allows DLITE to handle digitization ambiguities and errors better and robustly predict the distribution of cell-cell forces.

DLITE is robust to topological changes

Network topology or the structure of edges and vertices often display changes in time-series data. In Fig. 3 *D*, for example, there are two topological changes at time points 6 and 8 (edge labels 8 and 25, respectively) that result in differences between CellFIT and DLITE (Fig. 3, *E* and *F*), with DLITE showing better correlation to the ground truth. Handling of a time-ordered network requires the tracking of nodes, edges, and cells over time. This can be done in two ways; if, for example, a single edge ceases to exist at a certain time point, we can choose to either keep that edge label and assume that it has temporarily left the field of view or assign new edge labels ensuring that the lost edge label ceases to exist (63). Here, we choose the second option to condition the network based only on the immediately previous time point. Thus, an edge label that could not be tracked after a time point no longer exists and is assigned a new label. These rules were applied to nodes and cells as well.

If the observed topologies of a cellular network are constantly changing, how then does it affect inferred cell-cell forces? To study the effect of topological changes, we take advantage of the fact that decreasing the tension of two edges in a triple junction results in a decrease of the length of the third connected edge in Surface Evolver. Fig. 5 *A* shows an example time series in which edge label 15 disappears at time point 18. This single topological change leads to an ill-conditioned tension matrix (Eq. 2; Fig. 5, *B* and *C*). However, DLITE retains the correct distribution of tensions at time point 18 (see also Fig. 3 *E*, edge label 25 at time point 8, and Fig. S9 *A*) using the initial guess from previous time points. Although this specific network structure led to an ill-conditioned tension matrix after a single edge loss, this is not always the case. If the tension matrix is well conditioned after the topological change (Fig. 3 *E*, edge label 8 at time point 6, and Fig. S9 *B*), then CellFIT retains a good solution quality. However, Δtension is less smooth, and both the tension and Δtension still correlate better to the ground truth while using DLITE (Fig. 3, *E* and *F*; Fig. S9 *B*).

Another source of error in force-inference methods arises from temporal edge discontinuities when multiple edges appear and disappear between frames. To check the robustness of our method to temporal edge discontinuities, we simulated a field-of-view (FOV) drift within a single colony (Fig. 6 *A*). We did this by cropping out all cells outside a small FOV located in the lower left corner of the colony geometry. This FOV was then moved across the colony toward the upper right corner to generate a time series (Fig. 6 *A*). We performed this experiment at multiple speeds of frame drift so as to simulate a varying number of temporal edge discontinuities. For example, a slow FOV drift corresponds to the case with a few edge discontinuities between

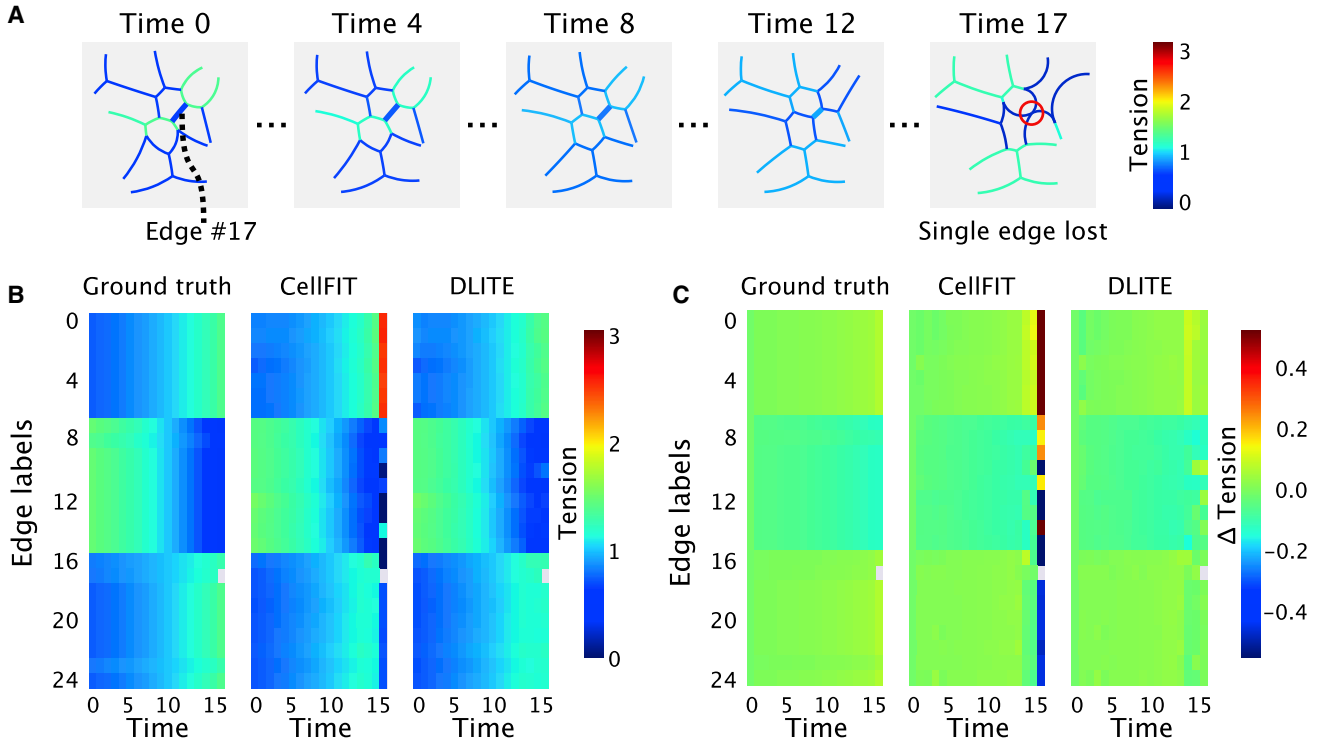

FIGURE 5 Reduced sensitivity to topological changes in DLITE. (*A*) Time series of a synthetic geometry containing 24 edges generated using Surface Evolver in which edge label 17 disappears at time 17 (*circled in red*). (*B*) A heat map of dynamic edge tensions for ground truth, CellFIT ($r = 0.75$), and DLITE ($r = 0.98$). DLITE shows reduced disruption to tension prediction on topological change and more closely matches the ground-truth tension. (*C*) A heat map of dynamic change (derivative of tension) in edge tensions for ground truth, CellFIT, and DLITE. To see this figure in color, go online.

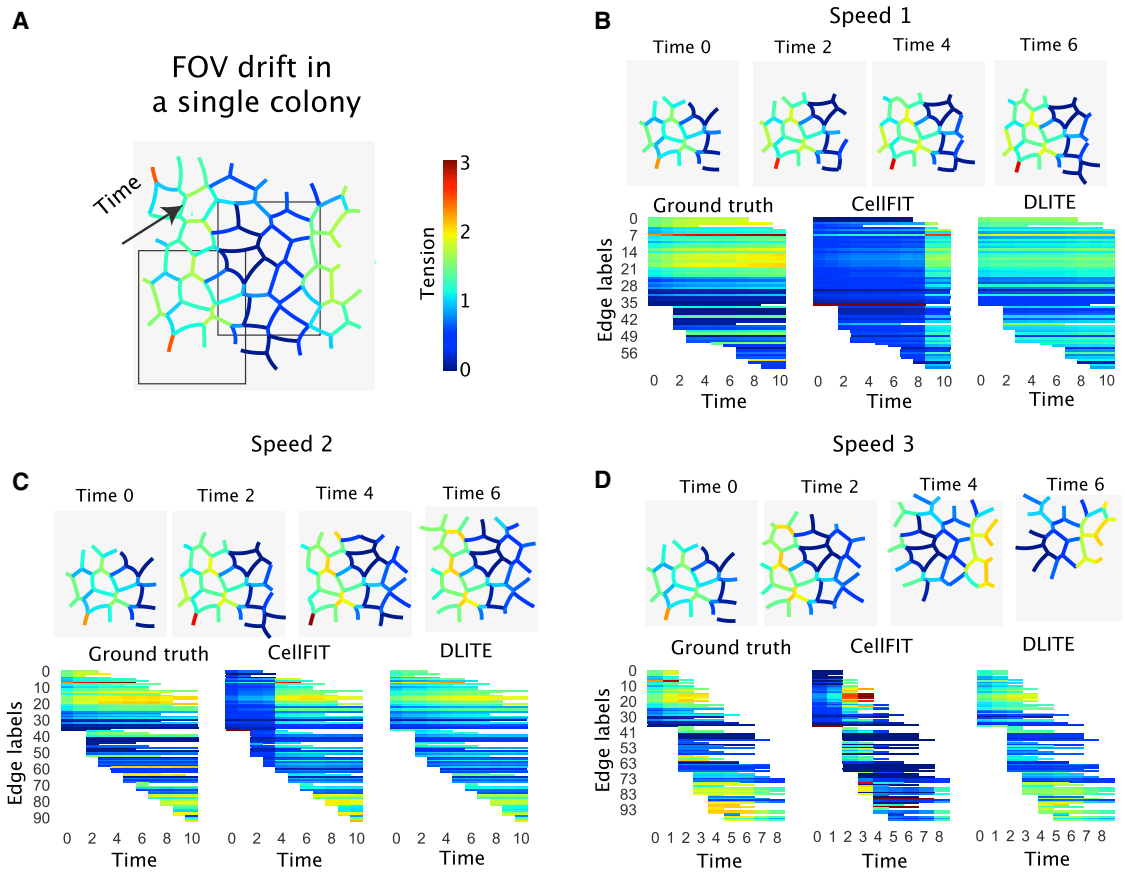

FIGURE 6 Reduced sensitivity to FOV (field-of-view) drift within a single colony when using DLITE compared to CellFIT. (*A*) FOV drift within a single synthetic geometry. The first frame is at the lower left corner. (*B–D*) Colony time series and heat map of dynamic edge tensions for ground truth, CellFIT, and DLITE generated via FOV drift with a small speed ((*B*) $r = 0.11$ versus $r = 0.83$), medium speed ((*C*) $r = 0.04$ versus $r = 0.87$), and large speed ((*D*) $r = 0.11$ versus $r = 0.87$). To see this figure in color, go online.

time steps (Fig. 6 *B*; Video S1) and a large FOV drift corresponds to the case in which multiple edges are discontinuous between time steps (Fig. 6, *C* and *D*; Videos S2 and S3). The FOV at time point 0 has a single edge that is disconnected from the rest of the colony (Fig. 6, *B–D*, time point 0), leading to tension errors during force inference using CellFIT. Such errors can be observed in time points 0–8 for speed 1 (Fig. 6 *B*), time points 0–4 for speed 2 (Fig. 6 *C*), and time points 0–2 and 4–7 for speed 3 (Fig. 6 *D*). These connectivity errors do not lead to errors when using DLITE (see Videos S1, S2, and S3 for DLITE predictions across time). In all cases, we observed a stable force inference when using DLITE, suggesting a reduced sensitivity to FOV drift.

Application to ZO-1 tight junctions

Finally, we applied DLITE to experimental images of colonies of hIPS cells (64). ZO-1 in hIPS cells was tagged at its endogenous locus with monomeric enhanced GFP (mEGFP) and visualized using a spinning confocal disk microscope (see Supporting Materials and Methods for more details). We chose this system because tight junctions (zonulae occludentes) are known to form a selective barrier, regulating paracellular diffusion through the spaces between cells. Injury of tight junctions can impair barrier function, leading to complications in lungs (65,66), kidneys (67), eyes (68), or the small intestine (69). The actin cytoskeleton plays an important role in the regulation of this barrier function (70) and is connected to the rest of the tight junction complex through ZO-1 proteins (71,72). Recent studies suggest that actin polymerization and transient Rho activation ("Rho flares") act to quickly restore barrier function upon localized ZO-1 loss at cell-cell contacts (73). Mechanical cues from the polymerization and branching of the actin network can lead to reshaping of tight junctions, resulting in varying barrier phenotypes.

Using a skeletonization of segmented GFP images, we predicted the evolution of intercellular forces in three different ZO-1 time series using both DLITE and CellFIT (Fig. 7, *A–C*). The edge lengths, angles, and curvatures of the synthetic colonies described in this study were chosen such that they qualitatively match well with the experimental data (Fig. S10). Because no ground truth is available in this

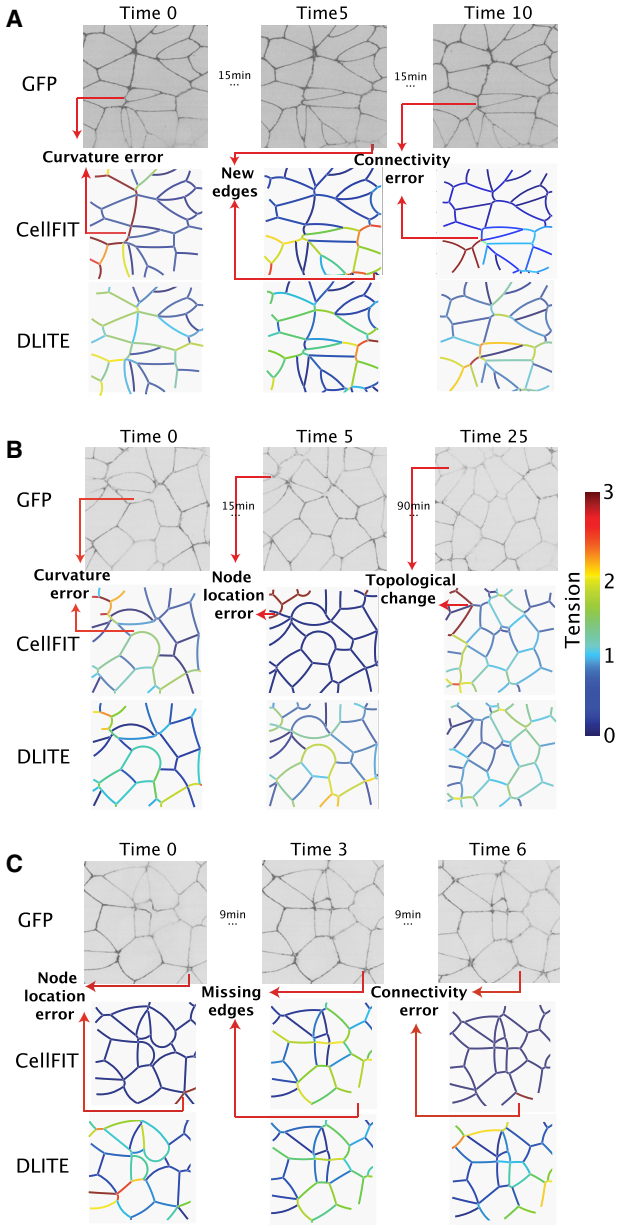

FIGURE 7 DLITE shows increased tension stability during tension inference in multiple time series of ZO-1-labeled hIPS cells. Example frames from three time series are shown in (*A*)–(*C*) and arranged as ZO-1 GFP (*upper*) and colony edge tensions predicted by CellFIT (*middle*) and DLITE (*lower*). Here, we use κ to denote the condition number of the tension matrix G_γ (Eq. 2). (*A*) DLITE shows increased stability to curvature errors (time 0, $\kappa = 69$), new edges (time 5, $\kappa = 32.5$), connectivity errors (time 10, $\kappa = 136$). (*B*) DLITE shows increased stability to curvature errors (time 0, $\kappa = 23$), node location errors (time 5, $\kappa = 10^{16}$), and topological changes (time 25, $\kappa = 46$). (*C*) DLITE shows increased stability to node location errors (time 0, $\kappa = 10^{16}$), missing edges (time 3, $\kappa = 31$), and connectivity errors (time 6, $\kappa = 10^{18}$). To see this figure in color, go online.

case, we determined the quality of predicted tensions using condition numbers (κ) of the tension matrix (Eq. 2) and tension residuals. We note that the relative distribution of tensions range from 0 to 3, such that the average tension is normalized to 1. The time interval between adjacent time points was 3 min. The example frames shown in Fig. 7, *A–C* are organized as raw GFP (upper), CellFIT-predicted tensions (middle), and DLITE-predicted tensions (lower). In every frame, we observed at least one kind of digitization error, leading to poor tension matrix condition numbers or tension residuals. Single-frame errors such as curvature errors (Fig. 7 *A*, time 0, $\kappa = 69$; Fig. 7 *B*, time 0, $\kappa = 23$), connectivity errors (Fig. 7 *A*, time 10, $\kappa = 136$; Fig. 7 *C*, time 6, $\kappa = 10^{18}$), node location errors (Fig. 7 *B*, time 5, $\kappa = 10^{16}$; Fig. 7 *C*, time 0, $\kappa = 10^{16}$) and time-series-specific errors such as new edges (Fig. 7 *A*, time 5, $\kappa = 32.5$), missing edges (Fig. 7 *C*, time 3, $\kappa = 31$), and topological changes (Fig. 7 *B*, time 25, $\kappa = 46$) result in loss of tension stability and errors (Fig. 7 *A*, CellFIT). Despite these digitization errors, DLITE shows increased tension stability (Fig. 7 *A*, DLITE), demonstrating its utility for experimental data sets as well. Heat maps of dynamic edge tension and change in edge tension (Δtension) for the time series in Fig. 7 are also shown in Fig. S11. The improved performance of DLITE is predicated on reduced tension residuals at every time point (Fig. S12). Importantly, the reduction in tension residuals is accompanied by a reduced dynamic change in edge tension (Δtension; Fig. S11), indicating a smoothness across time.

Interestingly, we observed an increase in tension adjacent to a dividing cell immediately after a mitotic event (Fig. 8 *A*, *red box*) in a time series of ZO-1 GFP with a single mitotic event at time point 14 (see Videos S4, S5, and S6 for selected edge tension tracks). This increase in tension post-mitosis was observed using both methods (Fig. 8 *C*, edge labels 3, 10, and 11) but only after the removal of digitization errors during a semimanual skeletonization process. This step was important to ensure non-poorly scaled CellFIT solutions, such as the ones at time points 2 and 13. As before, both the tension residuals (Fig. 8 *B*) and the dynamic change in tension (Δtension; Fig. 8, *D* and *E*) were reduced when using DLITE. The reduction in Δtension was determined to be sensitive to the time interval. The SD of Δtension across time was significantly reduced at a time lag of one frame (3 min) but showed no difference between methods for a time lag of five frames (15 min).

DISCUSSION

In this study, we have presented a new method, DLITE, which is based on a local optimization of tension residuals to compute dynamic cell-cell forces. We validated the predictive power of DLITE using synthetic geometries generated by Surface Evolver (55) and showed that DLITE performs better than the previous state-of-the-art method CellFIT when applied to time-series data. Importantly, this method incorporates a framework to track nodes, edges, and cells across time.

We demonstrated that DLITE is robust to digitization challenges common in time-series data such as poor estimates of edge angle, errors in node location, connectivity

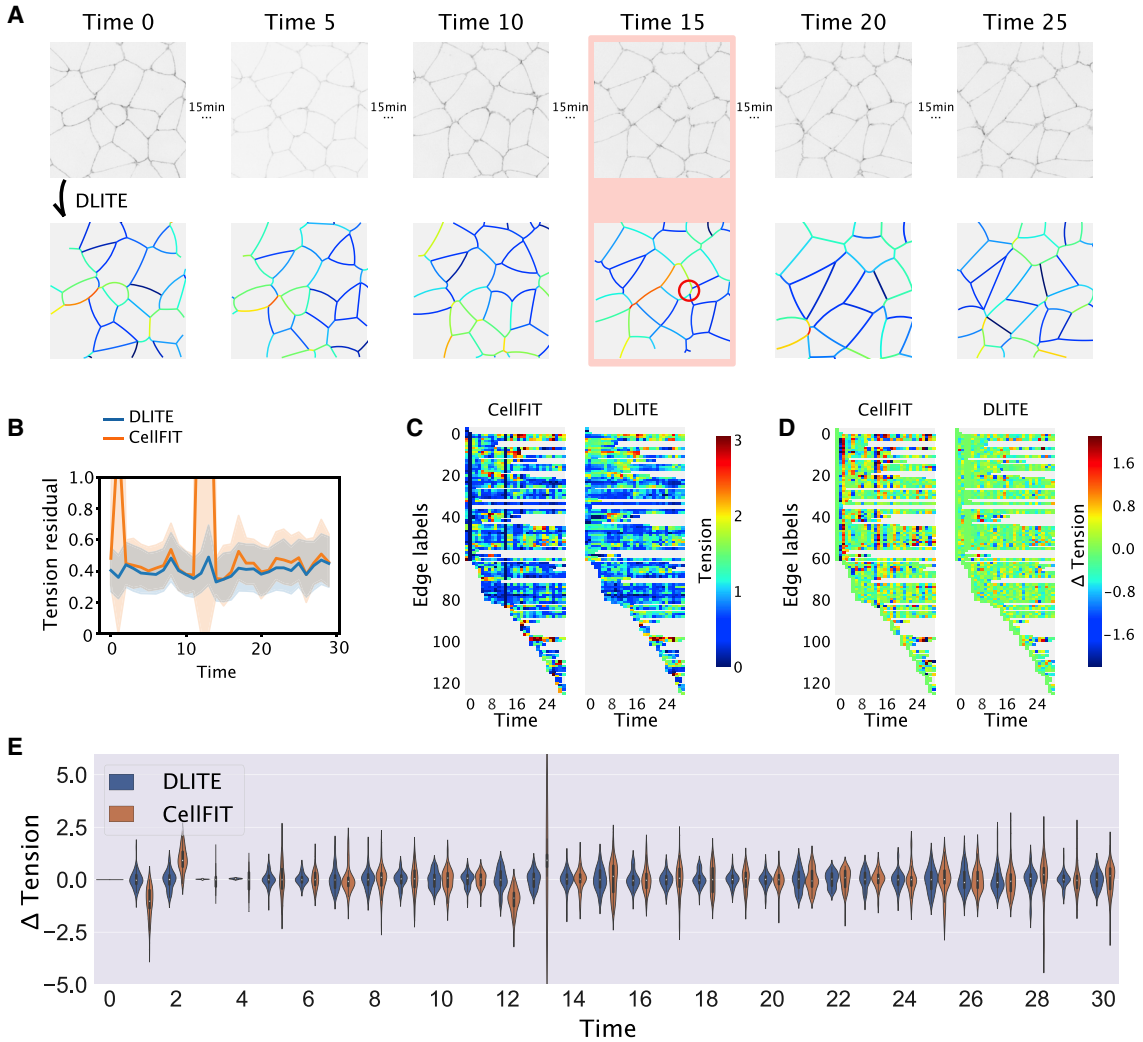

FIGURE 8 Dynamic cell-cell forces from a time series of ZO-1 tight junction locations in hIPS cells. DLITE shows reduced fluctuation in tension change, showing more temporally correlated tension predictions. (*A*) A time series of ZO-1 GFP images (*upper*) and dynamics of colony edge tension predicted by DLITE (*lower*). The following time points are shown: 0, 5, 10, 15, 20, and 25. Time 15 shows an increase in tension along a ridge in the middle of the colony after a mitotic event and the forming of a new edge (*circled in red*). The time interval between adjacent time points was 3 min. (*B*) Tension residuals at every time point showing an estimate of central tendency and corresponding confidence interval. (*C*) A heat map of dynamic edge tensions predicted by CellFIT and DLITE. (*D*) A heat map of dynamic change (derivative of tension) in edge tensions predicted by CellFIT and DLITE. (*E*) The distribution of Δtension (derivative of tension) at every time point for CellFIT and DLITE. To see this figure in color, go online.

errors, and topological changes that occur as cells move and encounter different neighbors. Finally, we applied DLITE to estimate edge tensions in multiple time series of ZO-1 tight junctions and showed improved stability in tension predictions and an increase in tension postmitosis. We indicated that DLITE displays a reduced Δtension compared to CellFIT, indicating greater temporal smoothness. We observed this reduction in three other scenes of the ZO-1 tight junction.

The need for dynamic force-inference tools to understand cell shape and colony rearrangement is driven by their applicability to morphogenic processes from wound healing to germ-band extension to colony reorganization (1–4). These processes rely on transient mechanical forces that are ideally detected by the extended nonperturbing observations for which DLITE is designed. Computing the dynamics of cell-cell forces via this computational framework complements experimental advances and enable data-driven estimation of intercellular forces, particularly as biological data sets grow in size.

Although useful, DLITE makes assumptions about the system that create limitations. Specifically, DLITE assumes 1) edges are circular arcs, 2) that tension is correlated from time point to time point, 3) that sufficient computational resources are available, and 4) that tensions and pressures in the system are homogeneous across interfaces. 1) The tensions calculated using DLITE depend on fitting circular arcs to every edge. This approximation breaks down if the

edge is not under sufficient tension or the cytoskeleton is strongly perturbing it inhomogeneously across the interface (74). Under these conditions, the inferred tensions will not approach the ground truth. 2) Using local optimization seeded with tensions from the previous time point assumes that the tensions are correlated across these time points. This is evidently true as the interframe interval approaches zero and evidently false as the same interval approaches infinity. DLITE's informed prior decreases in usefulness as we increase this interval or the timescale of our system's force variance decreases. 3) As the amount of biological data increases, implementation of DLITE must be optimized for computation speed in large colonies (Table 1). Global optimization routines at the first/zeroth time point can further slow down computation without providing substantial benefits. 4) Finally, without extensions beyond the current form, DLITE is not suitable for examining cases in which the actomyosin cortex is subject to substantial inhomogeneities or nonlinearities (8,74–77). Tracking local strains and including viscous damping can potentially incorporate inhomogeneities (78,79). This can be validated against Surface Evolver models utilizing local forces (80).

DLITE offers comparable tension inference to existing methods when applied to single time points, increased performance when applied across time points, increased stability in the face of segmentation challenges, and increased stability when applied to limited experimental data sets. Future use of DLITE will look at dynamic changes in cell-cell forces in larger data sets of ZO-1 tight junctions, allowing the visualization of cell-cell forces during large-scale colony reorganization.

SUPPORTING MATERIAL

Supporting Material can be found online at https://doi.org/10.1016/j.bpj.2019.09.034.

AUTHOR CONTRIBUTIONS

Designed research, R.V., M.M.M., C.D.W., and P.R.; Performed research, R.V. and C.D.W.; Contributed analytic tools, R.V. and C.D.W.; Analyzed the data, R.V., M.M.M., C.D.W., and P.R.; Wrote the article, R.V., M.M.M., C.D.W., and P.R.

ACKNOWLEDGMENTS

We thank the entire Allen Institute for Cell Science team, who generated and characterized the gene-edited hiPS cell lines and developed image-based assays used in this work. We especially thank the Allen Institute for Cell Science Assay Development team, particularly Irina Mueller for collecting the ZO-1 time series used here and Susanne Rafelski for invaluable discussions and advise. We thank the Allen Institute for Cell Science Animated Cell team and Daniel Toloudis specifically for providing the 3D rendering of ZO-1 cells used in Fig. 1. We thank Paul G. Allen, founder of the Allen Institute for Cell Science, for his vision, encouragement, and support. We also thank members of the P.R. lab and Dr. Matthew Akamatsu for comments and feedback.

This work was partially supported by Army Research Office W911NF1610411 and Office of Naval Research N00014-17-1-2628 to P.R.

REFERENCES

1. Heck, N., and R. Benavides-Piccione. 2015. Editorial: dendritic spines: from shape to function. *Front. Neuroanat.* 9:101.
2. Evans, N. D., C. Minelli, …, M. M. Stevens. 2009. Substrate stiffness affects early differentiation events in embryonic stem cells. *Eur. Cell. Mater.* 18:1–13, discussion 13–14.
3. Paulin, J. J., P. Haslehurst, …, F. A. Edwards. 2016. Large and small dendritic spines serve different interacting functions in hippocampal synaptic plasticity and homeostasis. *Neural Plast.* 2016:6170509.
4. Stevens, M. M., and J. H. George. 2005. Exploring and engineering the cell surface interface. *Science.* 310:1135–1138.
5. Calizo, R. C., A. Ron, …, R. Iyengar. 2018. Cell shape regulates subcellular organelle location to control short-term Ca^{2+} signal dynamics in VSMC. *bioRxiv* https://doi.org/10.1101/161950.
6. Ron, A., E. U. Azeloglu, …, R. Iyengar. 2017. Cell shape information is transduced through tension-independent mechanisms. *Nat. Commun.* 8:2145.
7. Hu, M., E. U. Azeloglu, …, L. J. Kaufman. 2017. A biomimetic gelatin-based platform elicits a pro-differentiation effect on podocytes through mechanotransduction. *Sci. Rep.* 7:43934.
8. Vasan, R., M. Akamatsu, …, P. Rangamani. 2018. Intracellular membrane trafficking: modeling local movements in cells. *In* Cell Movement: Modeling and Applications. M. Stolarska and N. Tarfulea, eds. Birkhäuser, pp. 259–301.
9. Brugués, A., E. Anon, …, X. Trepat. 2014. Forces driving epithelial wound healing. *Nat. Phys.* 10:683–690.
10. Sunyer, R., V. Conte, …, X. Trepat. 2016. Collective cell durotaxis emerges from long-range intercellular force transmission. *Science.* 353:1157–1161.
11. Serra-Picamal, X., V. Conte, …, X. Trepat. 2012. Mechanical waves during tissue expansion. *Nat. Phys.* 8:628–634.
12. du Roure, O., A. Saez, …, B. Ladoux. 2005. Force mapping in epithelial cell migration. *Proc. Natl. Acad. Sci. USA.* 102:2390–2395.
13. Ray, A., O. Lee, …, P. P. Provenzano. 2017. Anisotropic forces from spatially constrained focal adhesions mediate contact guidance directed cell migration. *Nat. Commun.* 8:14923.
14. Labernadie, A., T. Kato, …, X. Trepat. 2017. A mechanically active heterotypic E-cadherin/N-cadherin adhesion enables fibroblasts to drive cancer cell invasion. *Nat. Cell Biol.* 19:224–237.
15. Diz-Muñoz, A., D. A. Fletcher, and O. D. Weiner. 2013. Use the force: membrane tension as an organizer of cell shape and motility. *Trends Cell Biol.* 23:47–53.
16. Malinova, T. S., and S. Huveneers. 2018. Sensing of cytoskeletal forces by asymmetric adherens junctions. *Trends Cell Biol.* 28:328–341.
17. Tornavaca, O., M. Chia, …, M. S. Balda. 2015. ZO-1 controls endothelial adherens junctions, cell-cell tension, angiogenesis, and barrier formation. *J. Cell Biol.* 208:821–838.
18. Yano, T., H. Kanoh, …, S. Tsukita. 2017. Apical cytoskeletons and junctional complexes as a combined system in epithelial cell sheets. *Ann. N. Y. Acad. Sci.* 1405:32–43.
19. Borghi, N., and W. James Nelson. 2009. Intercellular adhesion in morphogenesis: molecular and biophysical considerations. *Curr. Top. Dev. Biol.* 89:1–32.
20. Chu, Y. S., W. A. Thomas, …, S. Dufour. 2004. Force measurements in E-cadherin-mediated cell doublets reveal rapid adhesion strengthened by actin cytoskeleton remodeling through Rac and Cdc42. *J. Cell Biol.* 167:1183–1194.
21. Trepat, X., and J. J. Fredberg. 2011. Plithotaxis and emergent dynamics in collective cellular migration. *Trends Cell Biol.* 21:638–646.

22. Leckband, D. E., Q. le Duc, …, J. de Rooij. 2011. Mechanotransduction at cadherin-mediated adhesions. *Curr. Opin. Cell Biol.* 23:523–530.

23. Rosenblatt, J., M. C. Raff, and L. P. Cramer. 2001. An epithelial cell destined for apoptosis signals its neighbors to extrude it by an actin- and myosin-dependent mechanism. *Curr. Biol.* 11:1847–1857.

24. Pilot, F., and T. Lecuit. 2005. Compartmentalized morphogenesis in epithelia: from cell to tissue shape. *Dev. Dyn.* 232:685–694.

25. Polacheck, W. J., and C. S. Chen. 2016. Measuring cell-generated forces: a guide to the available tools. *Nat. Methods.* 13:415–423.

26. Dufrêne, Y. F., T. Ando, …, D. J. Müller. 2017. Imaging modes of atomic force microscopy for application in molecular and cell biology. *Nat. Nanotechnol.* 12:295–307.

27. Hogan, B., A. Babataheri, …, J. Husson. 2015. Characterizing cell adhesion by using micropipette aspiration. *Biophys. J.* 109:209–219.

28. Diz-Muñoz, A., K. Thurley, …, O. D. Weiner. 2016. Membrane tension acts through PLD2 and mTORC2 to limit actin network assembly during neutrophil migration. *PLoS Biol.* 14:e1002474.

29. Dai, J., and M. P. Sheetz. 1999. Membrane tether formation from blebbing cells. *Biophys. J.* 77:3363–3370.

30. Colom, A., E. Derivery, …, A. Roux. 2018. A fluorescent membrane tension probe. *Nat. Chem.* 10:1118–1125.

31. Gayrard, C., and N. Borghi. 2016. Fret-based molecular tension microscopy. *Methods.* 94:33–42.

32. Grashoff, C., B. D. Hoffman, …, M. A. Schwartz. 2010. Measuring mechanical tension across vinculin reveals regulation of focal adhesion dynamics. *Nature.* 466:263–266.

33. Sugimura, K., P. F. Lenne, and F. Graner. 2016. Measuring forces and stresses in situ in living tissues. *Development.* 143:186–196.

34. Dembo, M., T. Oliver, …, K. Jacobson. 1996. Imaging the traction stresses exerted by locomoting cells with the elastic substratum method. *Biophys. J.* 70:2008–2022.

35. Engler, A. J., S. Sen, …, D. E. Discher. 2006. Matrix elasticity directs stem cell lineage specification. *Cell.* 126:677–689.

36. Balaban, N. Q., U. S. Schwarz, …, B. Geiger. 2001. Force and focal adhesion assembly: a close relationship studied using elastic micropatterned substrates. *Nat. Cell Biol.* 3:466–472.

37. Brodland, G. W., J. H. Veldhuis, …, M. S. Hutson. 2014. CellFIT: a cellular force-inference toolkit using curvilinear cell boundaries. *PLoS One.* 9:e99116.

38. Ishihara, S., and K. Sugimura. 2012. Bayesian inference of force dynamics during morphogenesis. *J. Theor. Biol.* 313:201–211.

39. Veldhuis, J. H., A. Ehsandar, …, G. W. Brodland. 2017. Inferring cellular forces from image stacks. *Philos. Trans. R. Soc. Lond. B Biol. Sci.* 372:20160261.

40. Alt, S., P. Ganguly, and G. Salbreux. 2017. Vertex models: from cell mechanics to tissue morphogenesis. *Philos. Trans. R. Soc. Lond. B Biol. Sci.* 372.

41. Brodland, G. W., V. Conte, …, M. Miodownik. 2010. Video force microscopy reveals the mechanics of ventral furrow invagination in Drosophila. *Proc. Natl. Acad. Sci. USA.* 107:22111–22116.

42. Ishihara, S., K. Sugimura, …, F. Graner. 2013. Comparative study of non-invasive force and stress inference methods in tissue. *Eur Phys J E Soft Matter.* 36:9859.

43. Chiou, K. K., L. Hufnagel, and B. I. Shraiman. 2012. Mechanical stress inference for two dimensional cell arrays. *PLoS Comput. Biol.* 8:e1002512.

44. Fruchterman, T. M., and E. M. Reingold. 1991. Graph drawing by force-directed placement. *Softw. Pract. Exper.* 21:1129–1164.

45. Beck, A., and A. Ben-Tal. 2006. On the solution of the Tikhonov regularization of the total least squares problem. *SIAM J. Optim.* 17:98–118.

46. Jones, E., T. Oliphant, and P. Peterson. 2014. SciPy: open source scientific tools for Python (SciPy Developers).

47. Wales, D. J., and J. P. Doye. 1997. Global optimization by basin-hopping and the lowest energy structures of Lennard-Jones clusters containing up to 110 atoms. *J. Phys. Chem. A.* 101:5111–5116.

48. Albert, P. J., and U. S. Schwarz. 2014. Dynamics of cell shape and forces on micropatterned substrates predicted by a cellular Potts model. *Biophys. J.* 106:2340–2352.

49. Graner, F., and J. A. Glazier. 1992. Simulation of biological cell sorting using a two-dimensional extended Potts model. *Phys. Rev. Lett.* 69:2013–2016.

50. Nagai, T., and H. Honda. 2001. A dynamic cell model for the formation of epithelial tissues. *Philos. Mag. B Phys. Condens. MatterStat. Mech. Electron. Opt. Magn. Prop.* 81:699–719.

51. Nagai, T., and H. Honda. 2009. Computer simulation of wound closure in epithelial tissues: cell-basal-lamina adhesion. *Phys. Rev. E Stat. Nonlin. Soft Matter Phys.* 80:061903.

52. Brodland, G. W., D. Viens, and J. H. Veldhuis. 2007. A new cell-based FE model for the mechanics of embryonic epithelia. *Comput. Methods Biomech. Biomed. Engin.* 10:121–128.

53. Chen, H. H., and G. W. Brodland. 2000. Cell-level finite element studies of viscous cells in planar aggregates. *J. Biomech. Eng.* 122:394–401.

54. Fozard, J. A., M. Lucas, …, O. E. Jensen. 2013. Vertex-element models for anisotropic growth of elongated plant organs. *Front. Plant Sci.* 4:233.

55. Brakke, K. A. 1992. The surface evolver. *Exp. Math.* 1:141–165.

56. Debnath, D., J. S. Gainer, …, K. T. Matchev. 2016. Edge detecting new physics the Voronoi way. *EPL.* 114:41001.

57. McQuin, C., A. Goodman, …, A. E. Carpenter. 2018. CellProfiler 3.0: next-generation image processing for biology. *PLoS Biol.* 16:e2005970.

58. Stylianidou, S., C. Brennan, …, P. A. Wiggins. 2016. SuperSegger: robust image segmentation, analysis and lineage tracking of bacterial cells. *Mol. Microbiol.* 102:690–700.

59. LeCun, Y., Y. Bengio, and G. Hinton. 2015. Deep learning. *Nature.* 521:436–444.

60. Ounkomol, C., S. Seshamani, …, G. R. Johnson. 2018. Label-free prediction of three-dimensional fluorescence images from transmitted-light microscopy. *Nat. Methods.* 15:917–920.

61. Attali, D., and A. Montanvert. 1997. Computing and simplifying 2D and 3D continuous skeletons. *Comput. Vis. Image Underst.* 67:261–273.

62. Kudelski, D., J.-L. Mari, and S. Viseur. 2010. 3D feature line detection based on vertex labeling and 2D skeletonization. *In* Proceedings of the 2010 Shape Modeling International Conference. IEEE Computer Society, pp. 246–250.

63. Blonder, B., T. W. Wey, …, A. Sih. 2012. Temporal dynamics and network analysis. *Methods Ecol. Evol.* 3:958–972.

64. Roberts, B., A. Haupt, …, R. N. Gunawardane. 2017. Systematic gene tagging using CRISPR/Cas9 in human stem cells to illuminate cell organization. *Mol. Biol. Cell.* 28:2854–2874.

65. Holgate, S. T. 2008. The airway epithelium is central to the pathogenesis of asthma. *Allergol. Int.* 57:1–10.

66. Meng, G., J. Zhao, …, J. X. Ruan. 2011. Injury of cell tight junctions and changes of actin level in acute lung injury caused by the perfluoroisobutylene exposure and the role of Myosin light chain kinase. *J. Occup. Health.* 53:250–257.

67. Smoyer, W. E., and P. Mundel. 1998. Regulation of podocyte structure during the development of nephrotic syndrome. *J. Mol. Med. (Berl.).* 76:172–183.

68. Rizzolo, L. J., S. Peng, …, W. Xiao. 2011. Integration of tight junctions and claudins with the barrier functions of the retinal pigment epithelium. *Prog. Retin. Eye Res.* 30:296–323.

69. Fries, W., E. Mazzon, …, G. Longo. 1999. Experimental colitis increases small intestine permeability in the rat. *Lab. Invest.* 79:49–57.

70. Mège, R. M., J. Gavard, and M. Lambert. 2006. Regulation of cell-cell junctions by the cytoskeleton. *Curr. Opin. Cell Biol.* 18:541–548.

71. Vasioukhin, V., and E. Fuchs. 2001. Actin dynamics and cell-cell adhesion in epithelia. *Curr. Opin. Cell Biol.* 13:76–84.

72. Tsukita, S., M. Furuse, and M. Itoh. 1999. Structural and signalling molecules come together at tight junctions. *Curr. Opin. Cell Biol.* 11:628–633.

73. Stephenson, R. E., T. Higashi, I. S. Erofeev, T. R. Arnold, M. Leda, A. B. Goryachev, and A. L. Miller. 2019. Rho flares repair local tight junction leaks. *Developmental Cell.* 48:445–459.

74. Alimohamadi, H., R. Vasan, …, P. Rangamani. 2018. The role of traction in membrane curvature generation. *Mol. Biol. Cell.* 29:2024–2035.

75. Liu, Z., J. L. Tan, …, C. S. Chen. 2010. Mechanical tugging force regulates the size of cell-cell junctions. *Proc. Natl. Acad. Sci. USA.* 107:9944–9949.

76. Maruthamuthu, V., B. Sabass, …, M. L. Gardel. 2011. Cell-ECM traction force modulates endogenous tension at cell-cell contacts. *Proc. Natl. Acad. Sci. USA.* 108:4708–4713.

77. Vasan, R., S. Rudraraju, …, P. Rangamani. 2019. A mechanical model reveals that non-axisymmetric buckling lowers the energy barrier associated with membrane neck constriction. *arXiv*, arXiv:1906.06443 https://arxiv.org/abs/1906.06443.

78. Lee, P., and C. W. Wolgemuth. 2011. Crawling cells can close wounds without purse strings or signaling. *PLoS Comput. Biol.* 7:e1002007.

79. Banerjee, S., K. J. Utuje, and M. C. Marchetti. 2015. Propagating stress waves during epithelial expansion. *Phys. Rev. Lett.* 114:228101.

80. Cardamone, L., A. Laio, …, A. DeSimone. 2011. Cytoskeletal actin networks in motile cells are critically self-organized systems synchronized by mechanical interactions. *Proc. Natl. Acad. Sci. USA.* 108:13978–13983.